

USP42 protects ZNRF3/RNF43 from R-spondin-dependent clearance and inhibits Wnt signalling

Nicole Giebel^{1,†} , Anchel de Jaime-Soguero^{1,†}, Ana García del Arco¹, Jonathan J M Landry² , Marlene Tietje^{3,4}, Laura Villacorta², Vladimir Benes², Vanesa Fernández-Sáiz^{3,4} & Sergio P Acebrón^{1,*} 

Abstract

The tumour suppressors RNF43 and ZNRF3 play a central role in development and tissue homeostasis by promoting the turnover of the Wnt receptors LRP6 and Frizzled (FZD). The stem cell growth factor R-spondin induces auto-ubiquitination and membrane clearance of ZNRF3/RNF43 to promote Wnt signalling. However, the deubiquitinase stabilising ZNRF3/RNF43 at the plasma membrane remains unknown. Here, we show that the USP42 antagonises R-spondin by protecting ZNRF3/RNF43 from ubiquitin-dependent clearance. USP42 binds to the Dishevelled interacting region (DIR) of ZNRF3 and stalls the R-spondin-LGR4-ZNRF3 ternary complex by deubiquitinating ZNRF3. Accordingly, USP42 increases the turnover of LRP6 and Frizzled (FZD) receptors and inhibits Wnt signalling. Furthermore, we show that USP42 functions as a roadblock for paracrine Wnt signalling in colon cancer cells and mouse small intestinal organoids. We provide new mechanistic insights into the regulation R-spondin and conclude that USP42 is crucial for ZNRF3/RNF43 stabilisation at the cell surface.

Keywords colorectal cancer; deubiquitination; EMT; LGR4/5/6; mouse intestinal organoids

Subject Categories Cancer; Post-translational Modifications & Proteolysis; Signal Transduction

DOI 10.15252/embr.202051415 | Received 27 July 2020 | Revised 16 February 2021 | Accepted 1 March 2021 | Published online 30 March 2021

EMBO Reports (2021) 22: e51415

See also: **G Colozza & B-K Koo** (May 2021)

Introduction

The Wnt/ β -catenin signalling pathway plays essential roles in embryonic development and tissue homeostasis (Niehrs, 2010; Clevers *et al.*, 2014). In particular, Wnt/ β -catenin signalling governs

stem cell maintenance in many tissues, and its misregulation is a common cause of tumour initiation, most notably in colorectal cancer (Nusse & Clevers, 2017; Bugter *et al.*, 2020).

The stability of the Wnt receptors LRP6 and Frizzled (FZD) has emerged as the main mechanism modulating Wnt/ β -catenin signalling in adult stem cells (de Lau *et al.*, 2014; Leung *et al.*, 2018; Fenderico *et al.*, 2019). The RING-type E3 ubiquitin-ligases ZNRF3 and RNF43 bind Dishevelled (DVL) and induce endocytosis and degradation of the Wnt receptors (Hao *et al.*, 2012; Koo *et al.*, 2012; Jiang *et al.*, 2015). The R-spondin family of secreted proteins (RSPO1–4) form a ternary complex with LGR4/5/6 and RNF43/ZNRF3 (Kazanskaya *et al.*, 2004; Kazanskaya *et al.*, 2008; Carmon *et al.*, 2011; de Lau *et al.*, 2011; Glinka *et al.*, 2011; Zebisch & Jones, 2015), which induces RNF43/ZNRF3 auto-ubiquitination and clearance from the plasma membrane (Hao *et al.*, 2012; Koo *et al.*, 2012; Hao *et al.*, 2016). Hence, R-spondin promotes the stabilisation of LRP6 and FZD at the cell surface, boosting the responsiveness to Wnt ligands (Kazanskaya *et al.*, 2004; de Lau *et al.*, 2011; Glinka *et al.*, 2011; Koo *et al.*, 2012).

During development, ZNRF3/RNF43 are required for embryonic patterning, sex determination, as well as limb morphogenesis (Harris *et al.*, 2018; Szenker-Ravi *et al.*, 2018; Chang *et al.*, 2020; Lee *et al.*, 2020). In adults, activation of Wnt signalling induces the expression of ZNRF3/RNF43 in stem cells, which form a negative feedback loop that prevents their unscheduled proliferation (Koo *et al.*, 2012; Koo *et al.*, 2015). This mechanism has been proved to be critical for the homeostasis of the intestinal tract and the adrenal gland (Koo *et al.*, 2012; Basham *et al.*, 2019), as well as for the growth and metabolic zonation of the liver (Planas-Paz *et al.*, 2016).

Loss of ZNRF3/RNF43 function is prevalent across different types of cancer (Hao *et al.*, 2016; Bugter *et al.*, 2020). For instance, truncating mutations in ZNRF3/RNF43 and activating translocations of R-spondin occur in 20% and 10% of colorectal tumours, respectively (Seshagiri *et al.*, 2012; Giannakis *et al.*, 2014; Bond *et al.*, 2016). Loss of ZNRF3/RNF43 activity leads to extensive cellular proliferation and metaplasia (Koo *et al.*, 2012; Koo *et al.*, 2015) and has been

1 Centre for Organismal Studies (COS), Heidelberg University, Heidelberg, Germany

2 Genomics Core Facility, European Molecular Biology Laboratory (EMBL), Heidelberg, Germany

3 Department of Medicine III, Klinikum rechts der Isar, Technical University of Munich, Munich, Germany

4 TranslaTUM, Center for Translational Cancer Research, Technical University of Munich, Munich, Germany

*Corresponding author. Tel: +49 6221 545257; E-mail: sergio.acebron@cos.uni-heidelberg.de

†These authors contributed equally to this work

associated with epithelial-to-mesenchymal transition (EMT) in various Wnt-associated tumours (Hao *et al*, 2016; Murillo-Garzon & Kypta, 2017), including in colorectal cancer (Gujral *et al*, 2014; Wang *et al*, 2016). In contrast to previously reported mutations in downstream Wnt regulators such as β -catenin or APC, alterations in the R-spondin/LGR/RNF43/ZNRF3 axis render tumour dependency on Wnt ligands (Jiang *et al*, 2013; Koo *et al*, 2015; Han *et al*, 2017). This growth factor addiction is currently being exploited in clinical trials by using small molecule inhibitors against Porcupine (PORCN) (Jung & Park, 2020), which is required for Wnt secretion (Jiang *et al*, 2013; Koo *et al*, 2015).

Protein ubiquitination is a dynamic post-translational modification that results from a tug-of-war between matching pairs of E3 ligases and deubiquitinating enzymes (DUBs) (Fraile *et al*, 2012; MacGurn *et al*, 2012). In transmembrane proteins, ubiquitination directs quality control, trafficking and removal from the plasma membrane (MacGurn *et al*, 2012). In particular, the E3 ligases ZNRF3/RNF43 catalyse their ubiquitination and plasma membrane clearance upon interaction with R-spondin and LGR4–6 (Hao *et al*, 2012), but the deubiquitinase stabilising ZNRF3/RNF43 at the plasma membrane remains unidentified.

Here, we show that USP42 protects ZNRF3/RNF43 from R-spondin- and ubiquitin-dependent clearance at the plasma membrane. Mechanistically, USP42 interacts with the Dishevelled interacting region (DIR) of ZNRF3 and stalls the ZNRF3/LGR/RSPO complex. Accordingly, USP42 promotes the turnover of the Wnt receptors LRP6 and FZD and inhibits Wnt/ β -catenin signalling. Furthermore, we show that USP42 functions as a roadblock for cell proliferation, survival and EMT in colon cancer cells by inhibiting paracrine Wnt signalling. Finally, we report that genetic ablation of *Usp42* confers Wnt hypersensitivity to mouse small intestinal organoids. Our work reveals how ZNRF3 and RNF43 are stabilised at the plasma membrane and provides mechanistic insights on the modulation of the stem cell factors LGR4 and R-spondin.

Results

USP42 inhibits Wnt signalling by deubiquitinating ZNRF3

R-spondin proteins promote the auto-ubiquitination and membrane clearance of the E3 ligase ZNRF3/RNF43 (Hao *et al*, 2012; MacGurn *et al*, 2012), which is a key event for Wnt signalling modulation (Hao *et al*, 2012; Koo *et al*, 2012; Koo *et al*, 2015; Zebisch & Jones, 2015). However, the DUB responsible for ZNRF3/RNF43 deubiquitination and membrane stabilisation remains unknown (Fig 1A).

To identify a potential DUB regulating ZNRF3/RNF43, we performed a DUB small interfering RNA (siRNA) screen in HEK293T cells using the Wnt reporter assay (TOPflash) as a readout and identified USP42 among the candidates (Fig 1B and [Extended version] EV1A). *USP42* encodes a protein of 145 kDa with no clear structural features except its deubiquitinase (USP) domain, and a predicted monopartite nuclear localisation signal (NLS) (Fig 1C). USP42 localises to the cytoplasm, plasma membrane and nucleus (Fig 1D). Nuclear USP42 has been shown to deubiquitinate and stabilise H2B, as well as p53 in response to genotoxic stress (Hock *et al*, 2011; Hock *et al*, 2014).

Knockdown of USP42 in wt HEK293T cells by three independent siRNAs increased Wnt3a-induced TOPflash activity by > 2-fold

(Fig 1B and E). Critically, knockdown of USP42 did not upregulate Wnt reporter activity in ZNRF3/RNF43 double knockout HEK293T cells (Fig 1F), indicating a requirement of the E3 ligases for USP42 activity in Wnt signalling. To further assess USP42 function in Wnt signalling, we performed additional epistasis experiments. Knockdown of USP42 cooperated with the four R-spondin proteins (RSPO1–4) in Wnt reporter assays (Fig 1G), and boosted signalling induced by the ligand-receptor complex (Wnt1/LRP6/FZD8), but not by β -catenin (Fig 1H). Taking together, these data indicate that USP42 is a novel negative regulator of R-spondin and Wnt/ β -catenin signalling, functioning at the receptor level through RNF43/ZNRF3.

We next examined whether USP42 regulates ZNRF3 and RNF43 ubiquitination. We immunoprecipitated ZNRF3 under denaturing conditions and found that knockdown of USP42 increased its poly-ubiquitination (Fig 1I). Conversely, ectopic expression of USP42 erased the ubiquitin chains from ZNRF3 and RNF43 (Figs 1J and EV1B, IPs) and resulted in the accumulation of non-ubiquitinated ZNRF3 or RNF43 (Figs 1K and EV1B, inputs). To examine whether USP42 interacts with ZNRF3/RNF43, we performed co-immunoprecipitation (co-IP) experiments. GFP-USP42 co-precipitated ZNRF3, but not the component of the β -destruction complex AXIN1 (Fig 1K). On the other hand, the positive control GFP-DVL1 co-precipitated both ZNRF3 and AXIN1 (Fig 1K), as previously described (Bilic *et al*, 2007; Jiang *et al*, 2015). Additional co-IP experiments revealed that USP42 also interacted with RNF43 (Fig EV1C).

As in the case of ZNRF3, ectopic expression of USP42 in HEK293T cells inhibited the Wnt reporter signal induced by any of the four R-spondin proteins (RSPO1–4) (Fig 1L). Importantly, expression of the catalytically inactive mutant USP42^{C120A} did not inhibit Wnt reporter activity (Fig 1L). Furthermore, expression of USP42, but not USP42^{C120A} inhibited Wnt reporter assays induced by Wnt3a or by components of the LRP6 signalosome (Wnt1/LRP6/FZD8 and Dvl1), but not by β -catenin (Fig EV1D).

Finally, we generated USP42 KO HEK293T cells (Fig EV1E), which displayed higher TOPflash activation than the parental cells upon Wnt3a treatment (Fig 1M). Importantly, USP42 KO-induced Wnt activity was blocked by ectopic expression of RNF43/ZNRF3 or USP42, but not by USP42^{C120A} (Fig 1M). Taking these results together, we conclude that USP42 functions in Wnt signalling by deubiquitinating ZNRF3 and RNF43.

Cytoplasmic USP42 binds the Dishevelled interacting region of ZNRF3

We generated various USP42 and ZNRF3 deletion constructs to identify which domains participate in their functional interaction (Fig 2A). Deletion of the predicted NLS or the C-terminal domain of USP42 increased their cytoplasmic distribution compared to wild-type (wt) USP42 in HEK293T cells (Fig 2B). USP42 Δ NLS and USP42 Δ C co-precipitated ZNRF3 (Fig 2C) and inhibited Wnt signalling in reporter assays (Fig 2D) in a similar way as wt USP42. USP42 Δ N and USP42^{C120A} neither co-precipitated ZNRF3 nor reduced Wnt reporter assay activity (Fig 2C and D). Additional co-IP experiments with truncated ZNRF3 constructs revealed that USP42 requires the ZNRF3 Dishevelled interacting region (DIR) for its functional interaction (Fig 2E). Interestingly, ectopic expression of USP42 did not affect DVL2 binding to ZNRF3 (Fig 2F), suggesting that they do not compete for binding within the large ZNRF3 DIR

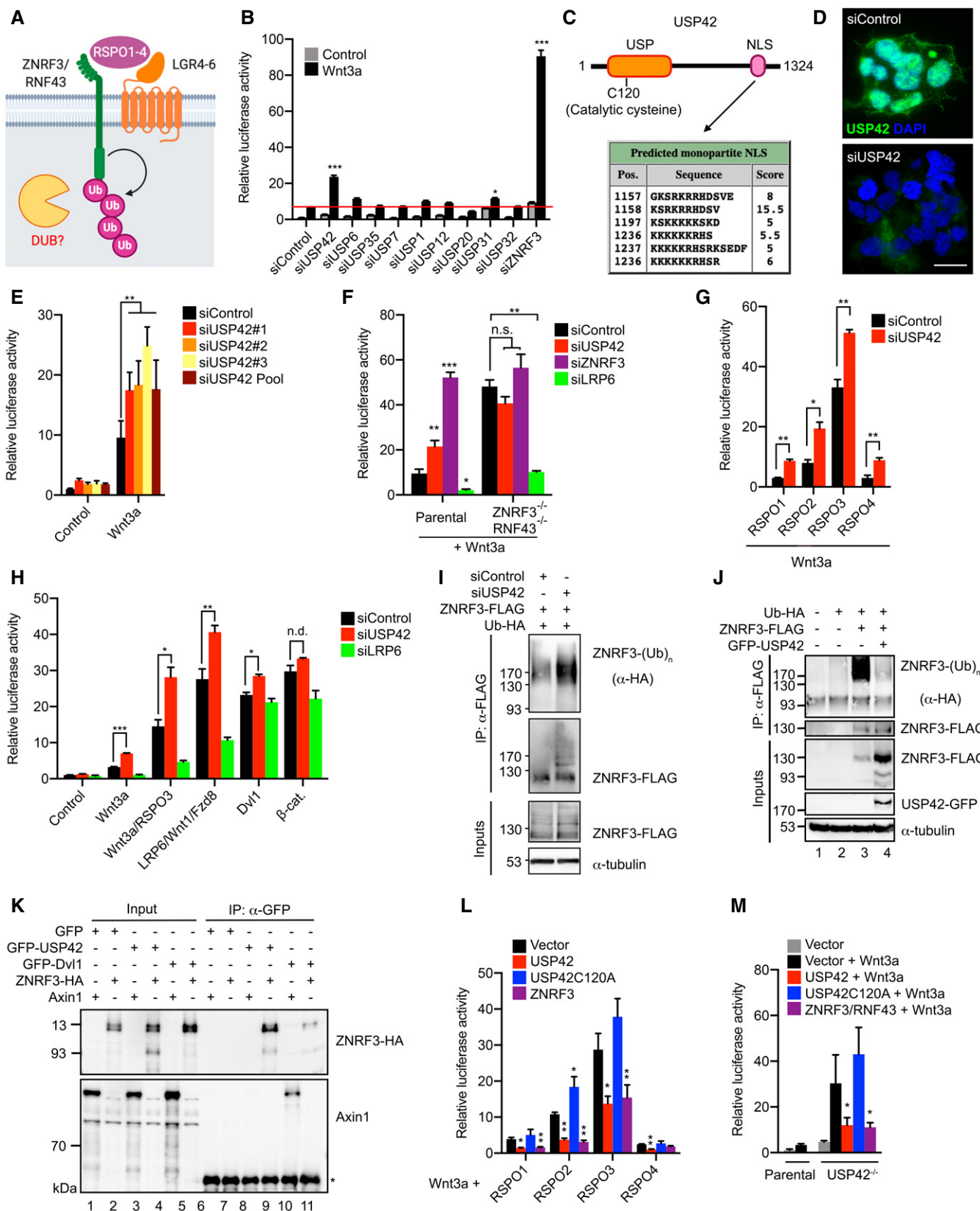


Figure 1.

Figure 1. USP42 deubiquitinates ZNRF3 and inhibits Wnt/ β -catenin signalling.

- A Scheme of the R-spondin complex with ZNRF3 and LGR, which promotes auto-ubiquitination and clearance of ZNRF3. The deubiquitinase (DUB) that stabilises ZNRF3 remains unknown.
- B Example of a TOPflash reporter assay used to screen for DUBs regulating Wnt signalling. Cells were transfected in triplicates with the single siRNAs against the indicated DUBs or the positive control ZNRF3 and stimulated with control or Wnt3a conditioned media.
- C Scheme showing the predicted protein organisation of USP42, including the catalytic cysteine of the ubiquitin-specific protease (USP) domain, and the predicted monopartite nuclear localisation signals (NLS) as displayed by NLS mapper (http://nls-mapper.iab.keio.ac.jp/cgi-bin/NLS_Mapper_form.cgi).
- D Representative immunofluorescence microscopy images showing endogenous USP42 (green) in HEK293T cells transfected with the indicated siRNAs from $n = 3$ independent experiments. Scale bar = 10 μ m.
- E–H TOPflash reporter assays in HEK293T cells stimulated with either control, Wnt3a, Wnt3a and RSPO1–4 conditioned media, or by transfection with the indicated constructs. Where indicated, cells were co-transfected with the indicated siRNAs. In (E), 3 independent siRNAs or a siRNA pool against USP42 were used. In (F), Parental wt HEK293T and ZNRF3^{-/-}/RNF43^{-/-} HEK293T cells were used.
- I, J Ubiquitination of ZNRF3 in HEK293T cells transfected with ubiquitin-HA (Ub-HA). Cells were co-transfected with siUSP42 (I) or GFP-USP42 (J). Cells were treated for 6 h with 10 μ M MG132 and 5 nM Bafilomycin A1 to prevent ZNRF3-Ub degradation. Ubiquitinated ZNRF3 was isolated by immunoprecipitation (IP) under denaturing conditions and analysed in Western blots with anti-HA antibodies.
- K Representative co-immunoprecipitation experiments in HEK293T cells that were transfected with GFP-USP42 or the indicated GFP-tagged control, together with the stated Wnt signalling component ($N = 3$ independent experiments). IgG heavy chain is indicated with an asterisk. Dvl1 functions as a positive control that binds both ZNRF3 and Axin1.
- L, M TOPflash reporter assays in HEK293T cells stimulated with either control, Wnt3a, Wnt3a and RSPO1–4 conditioned media, or by transfection with the indicated constructs. HEK293T, Parental HEK293T and USP42^{-/-} HEK293T cells were transfected with wt USP42, the catalytically inactive mutant USP42^{C120A}, ZNRF3 or ZNRF3/RNF43.

Data information: Data are displayed as mean \pm SD and show one representative of $n \geq 3$ independent experiments with three biological replicates. Statistical significance was calculated by one-way ANOVA analyses with Tukey correction and defined as * $P < 0.05$, ** $P < 0.01$, *** $P < 0.001$, or n.s.: not significant.

region (346–528 aa) (Jiang *et al.*, 2015). We conclude that cytoplasmic and catalytically active USP42 interacts with the ZNRF3 DIR (Fig 2G), which is emerging as a key modulatory domain of the E3 ligase (Jiang *et al.*, 2015; Chang *et al.*, 2020; Spit *et al.*, 2020; Tsukiyama *et al.*, 2020).

USP42 antagonises R-spondin and promotes Wnt receptor turnover

ZNRF3/RNF43 auto-ubiquitination promotes its turnover from the membrane (Hao *et al.*, 2012; Hao *et al.*, 2016). To assess whether USP42 stabilises ZNRF3/RNF43 directly at the plasma membrane, we performed cell surface protein biotinylation assays (Fig 3A, scheme). Expression of USP42 reduced the ubiquitination of ZNRF3 and RNF43 at the plasma membrane (Fig 3A, 2nd IP, lanes 3–4 and lanes 7–8, respectively). Accordingly, USP42 strongly increased ZNRF3 and RNF43 residence at the plasma membrane (Fig 3A, 1st IP, lanes 3–4 and lanes 7–8, respectively). Next, we investigated whether USP42 also protects ZNRF3/RNF43 from R-spondin. In the presence of LGR4, RSPO1 reduced the protein levels of mature ZNRF3 (Fig 3B, input: lanes 1,3, upper bands). Importantly, RSPO1 stimulated the interaction between ZNRF3 and USP42 Δ NLS (Fig 3B, IP: lanes 2,4), which rescued RSPO1-dependent clearance of ZNRF3 (Fig 3B, input: lanes 3,4).

To obtain further mechanistical insights on the ZNRF3 regulation by USP42, we analysed the formation the ternary complex between ZNRF3, R-spondin and LGR4. As previously described (Hao *et al.*, 2012), catalytically inactive ZNRF3 (ZNRF3 Δ Ring) co-precipitated LGR4, and this interaction was enhanced in the presence of RSPO3 (Fig 3C). Interestingly, USP42 interaction with ZNRF3 increased ternary complex formation (Fig 3C). These results suggest that ZNRF3 ubiquitination functions as release signal from R-spondin/LGR4, which allows USP42 to stall the ternary complex. This is supported by the fact that full-length ZNRF3, which displays high levels of auto-ubiquitination, did not form a stable complex with LGR4 (not shown and (Hao *et al.*, 2012)). Furthermore, our results showing that USP42 interacts with catalytically inactive ZNRF3

(ZNRF3 Δ Ring) (Figs 2E and 3C) support the possibility of additional E3 ligases contributing to ZNRF3 ubiquitination. In that respect, recent evidence pointed towards β -TrCP as a contributing E3 ligase for ZNRF3 turnover (Ci *et al.*, 2018).

Taking together, these results indicate that USP42 forms a tug-of-war with R-spondin and LGR4 to control ZNRF3/RNF43 ubiquitination and plasma membrane residence (Fig 3D).

Given the prominent role of ZNRF3 and RNF43 at the plasma membrane promoting Wnt receptor turnover, we next examined whether USP42 impacts FZD and LRP6 protein levels (Fig 3D). Ectopic expression of USP42 or ZNRF3 in HEK293T cells increased FZD5 clearance from the plasma membrane (Fig 3E) and reduced total FZD5 protein levels (Fig 3F). Furthermore, USP42 cooperated with ZNRF3 in clearing FZD8 (Fig 3G). Finally, knockdown of USP42 in HEK293T increased endogenous LRP6 protein levels, both in basal conditions and upon RSPO3 treatment (Fig 3H). We conclude that USP42 assists ZNRF3/RNF43 to promote Wnt receptor turnover.

USP42 is a roadblock for paracrine Wnt signalling in colorectal cancer cells

We noticed that *USP42* mRNA is often overexpressed in colorectal cancer (Fig 4A) (Cancer Genome Atlas, 2012). Furthermore, USP42 protein levels are elevated in several colon cancer cell lines, including HCT116 and RKO (The Protein Expression Atlas). Interestingly, colon cancer cells rely on paracrine Wnt signalling for their maintenance, even in the presence of downstream mutations in APC and β -catenin (Voloshanenko *et al.*, 2013). Hence, we decided to explore whether USP42 control of the Wnt receptors modulates paracrine Wnt signalling in colon cancer cells.

First, we analysed whether USP42 regulates the Wnt receptors in HCT116 cells. Knockdown of USP42 in HCT116 cells increased the surface levels of endogenous LRP6, including upon R-spondin treatment (Fig 4B and C). Accordingly, knockdown of USP42 in HCT116 cells promoted paracrine Wnt signalling activity in TOPflash reporter assays (Figs 4D and EV2A) and boosted Wnt3a-

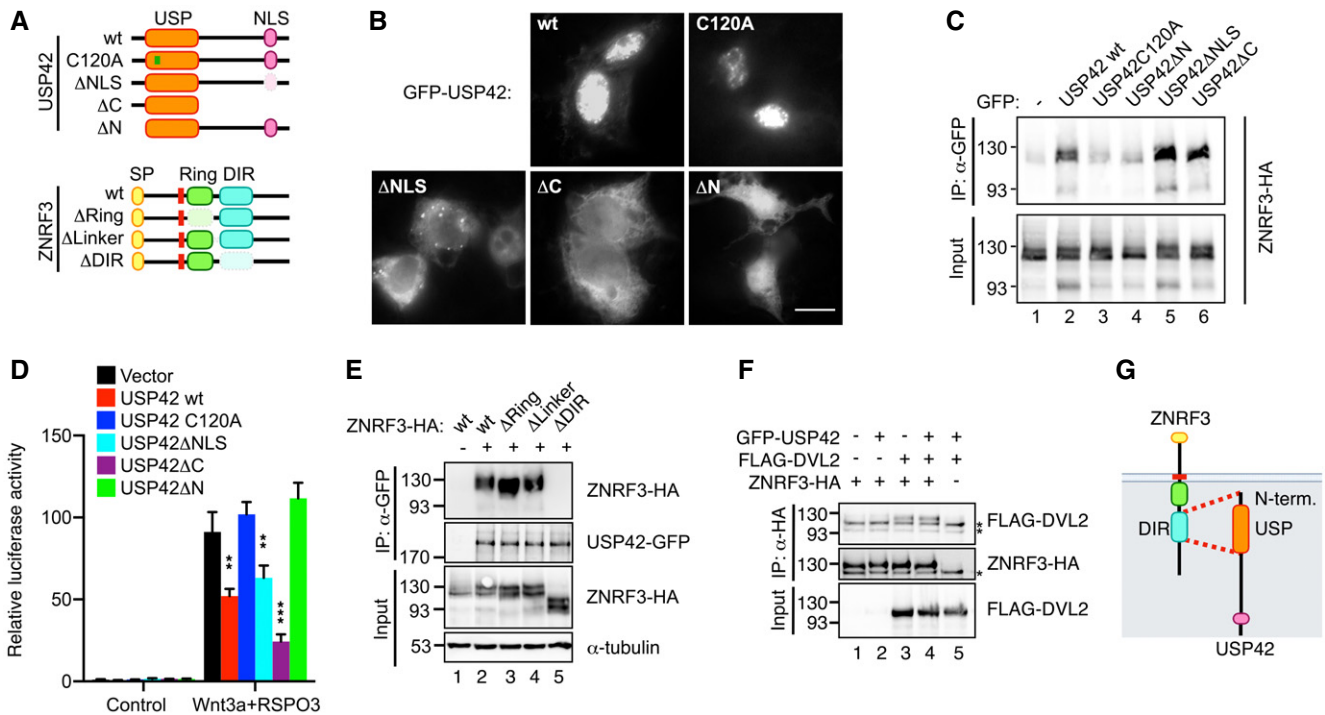


Figure 2. Cytoplasmic USP42 functionally interacts with the Dishevelled interacting region of ZNRF3.

- A** Scheme showing the GFP-USP42 and ZNRF3-HA constructs generated for this study. Note that ZNRF3ΔC did not express properly, possibly due to misfolding at the ER.
- B** Immunofluorescence microscopy showing HEK293T cells transfected with USP42 constructs from (A). Note that depletion of the putative NLS or the whole C-terminal domain containing the NLS leads to increased cytoplasmic expression of USP42. Representative images are shown. Scale bar = 10 μm.
- C** Co-immunoprecipitation experiments in HEK293T cells transfected with the constructs shown in (A). Representative blots of $n \geq 3$ independent experiments are shown.
- D** TOPflash reporter assay in HEK293T cells upon overexpression of the USP42 constructs shown in (A) or an empty vector. Cells were stimulated with control or Wnt3a and RSPO3 conditioned medium. Data are displayed as mean \pm SD and show one representative of $n = 3$ independent experiments with three biological replicates. Statistical significance was calculated by one-way ANOVA analyses with Tukey correction and defined as $^{**}P < 0.01$, $^{***}P < 0.001$, or n.s.: not significant.
- E, F** Co-immunoprecipitation experiments in HEK293T cells transfected with the constructs shown in (A). In (F), cells were co-transfected with DVL2 as indicated. Unspecific bands resulting from antibody cross-reaction are marked with asterisks. Representative blots of $n \geq 3$ independent experiments are shown.
- G** Scheme showing the proposed interacting regions of USP42 and ZNRF3.

dependent activation of the pathway (Fig 4D). Furthermore, siUSP42 upregulated the expression of the stem cell Wnt target gene *LGR5* in HCT116 cells (Fig 4E) and cooperated with Wnt3a to upregulate classical Wnt target *AXIN2* (Fig 4F).

USP42 has been shown to regulate p53 response upon genotoxic stress in colorectal cancer cells (Hock *et al.*, 2011). Importantly, knockdown of p53 did not impact Wnt reporter assays in HCT116 cells (Fig EV2B). However, both siUSP42 and siTP53 inhibited p53-reporter assays (Fig EV2C) and prevented cell cycle arrest at G1/S upon genotoxic stress in HCT116 cells (Fig EV2D), as described previously (Hock *et al.*, 2011). We conclude that USP42 inhibits Wnt signalling in HCT116 cells by destabilising the Wnt receptors, independently of its roles in p53 response to genotoxic stress.

Loss of RNF43/ZNRF3 activity is associated with cancer cell proliferation, survival and EMT through the activation of paracrine Wnt signalling (Fig 5A) (Koo *et al.*, 2012; Gujral *et al.*, 2014; Koo *et al.*, 2015; Hao *et al.*, 2016; Wang *et al.*, 2016; Murillo-Garzon & Kypta, 2017). To investigate whether USP42 is also involved in these cellular processes, we first performed bulk-RNA sequencing of HCT116 cells upon siUSP42 (Dataset EV1A-B). Gene Ontology (GO) cluster

analysis of the differentially upregulated genes upon USP42 silencing revealed enrichment of factors regulating cell cycle progression, Wnt signalling, protein ubiquitination and DNA replication (Fig EV3A–C and Dataset EV1C-E). Notably, knockdown of USP42 upregulated most of the 45 genes included in the intestinal stem cell proliferation signature (Merlos-Suarez *et al.*, 2011) (Fig 5B and Dataset EV1F). In addition, knockdown of USP42 downregulated epithelial genes and upregulated mesenchymal genes from the EMT gene signature in cancer ($N = 171$ genes) (Rokavec *et al.*, 2017) (Fig 5C and Dataset EV1G). Hence, we explored whether USP42 regulates cell proliferation, survival and EMT via paracrine Wnt signalling.

In agreement with our RNA-sequencing results (Fig 5C), knockdown of USP42 induced morphological changes in HCT116 cells, including a shift from cobblestone-like to elongated phenotype and loss of cell–cell contact (Fig 5D), which are characteristics of EMT (Thiery & Sleeman, 2006; Roger *et al.*, 2010; Nieto *et al.*, 2016). A key event for EMT is the downregulation of the cell–cell adhesion protein E-cadherin (Cano *et al.*, 2000; Thiery & Sleeman, 2006). HCT116 cells presented high levels of E-cadherin at their plasma membranes, which were erased upon USP42 knockdown with four

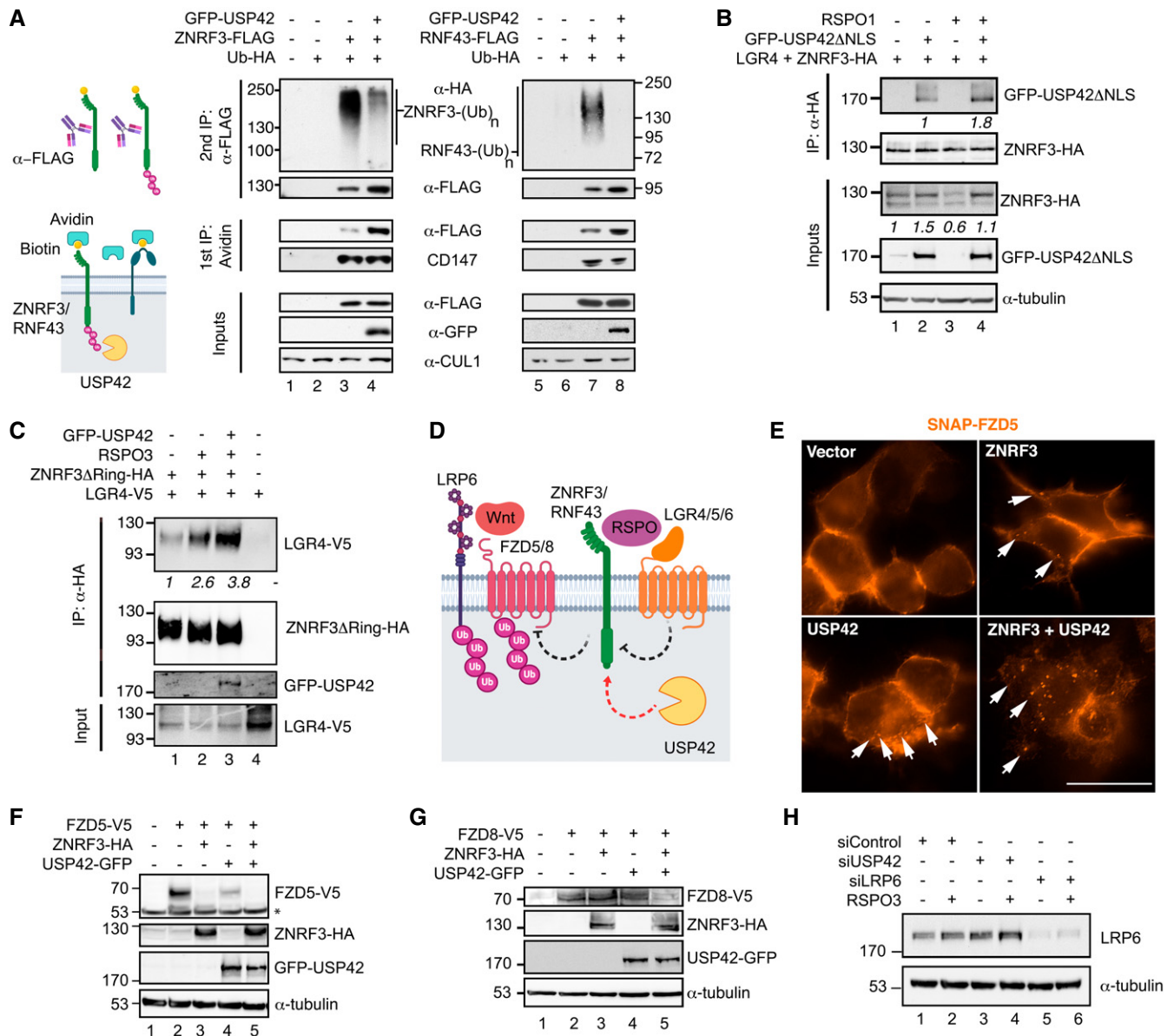


Figure 3. USP42 antagonises R-spondin/LGR and promotes FZD and LRP6 protein turnover.

- A** Cell surface biotinylation assay performed in HEK293T cells transfected as indicated and treated with 10 μ M MG132 to prevent proteasomal degradation. Consecutive immunoprecipitations were carried out as indicated in the scheme. The avidin pulldown was carried out under denaturing conditions (1st IP). The unrelated receptor CD147 was used as loading control for the avidin pulldown, and CUL1 for the total input of cell lysate.
- B, C** Co-immunoprecipitation experiments in HEK293T cells transfected with the indicated constructs and treated for 6 h with Bafilomycin A1. Cells were co-treated with RSPO1 (**B**) or RSPO3 (**C**) conditioned medium. In (**B**), co-immunoprecipitated cytoplasmic USP42 (USP42 Δ NLS) protein levels were quantified relative to immunoprecipitated ZNRF3. ZNRF3 levels in the input were quantified relative to tubulin. In (**C**), co-precipitated LGR4 protein levels were quantified relative to immunoprecipitated ZNRF3 Δ Ring. Representative blots of $n = 3$ independent experiments are shown.
- D** Scheme showing the proposed function for USP42 towards ZNRF3.
- E** Immunofluorescence microscopy of HEK293T cells transfected with SNAP-FZD5 and the indicated constructs. Cells were incubated with SNAP-surface-549 for 15 min and chased for another 10 minutes prior fixation. Representative images from one out of two independent experiments are shown. The white arrows show SNAP-FZD5 undergoing plasma membrane clearance. Scale bar = 20 μ m.
- F, G** Western blots of lysates from HEK293T cells transfected with the indicated constructs. The asterisk marks an unspecific band. Representative blots from at least three independent experiments are shown.
- H** Western blots of lysates from HEK293T cells transfected with the indicated siRNAs. Where indicated, cells were treated for 6 h with RSPO3 conditioned medium. Representative blots from $n = 4$ independent experiments are shown.

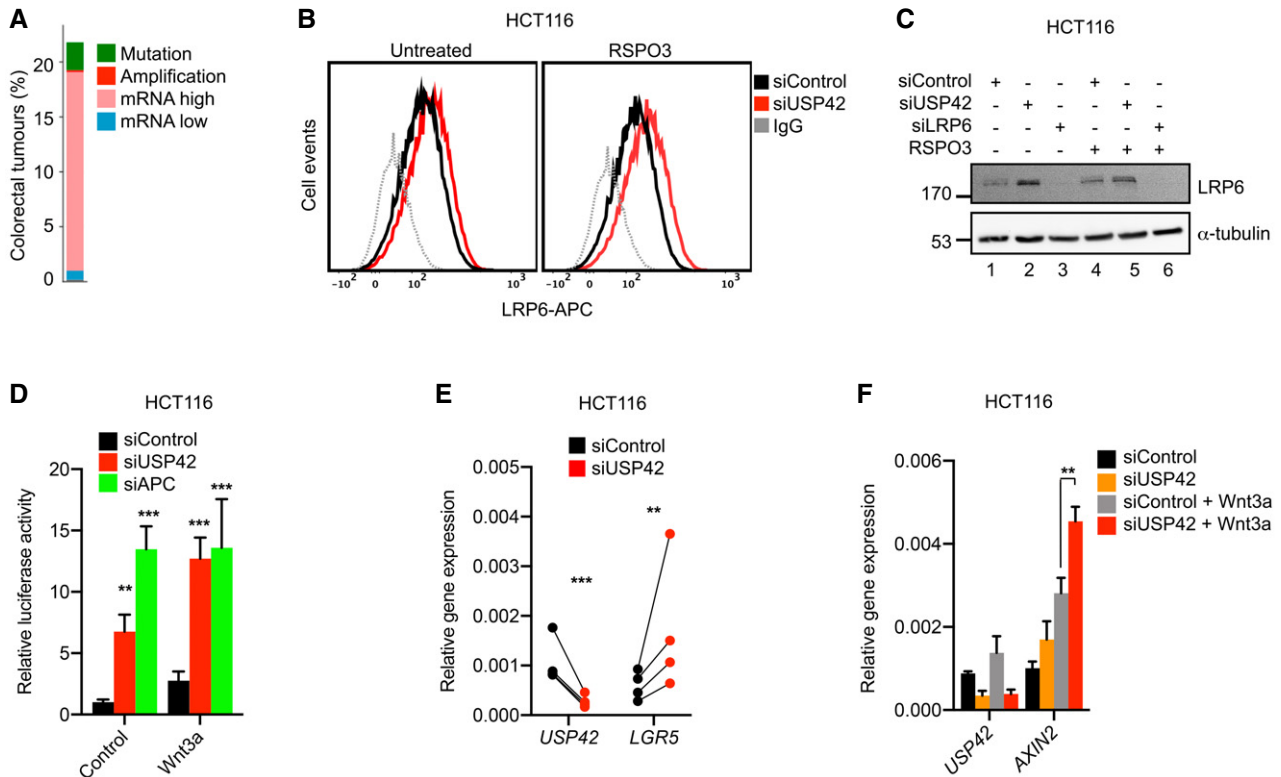


Figure 4. USP42 inhibits paracrine Wnt signalling in colorectal cancer cells.

- A USP42 alterations in colorectal adenocarcinoma (Cancer Genome Atlas, 2012) ($n = 524$). Information was retrieved from the cBioPortal in 2017, and updated as displayed in 03/2020.
- B FACS analyses of cell surface LRP6 protein levels in HCT116 cells upon knockdown of USP42. Cells were untreated (left panel) or treated with RSPO3 for 12 h (right panel). The grey dotted line in both panels shows background signal upon staining with control IgGs. Representative panels from one out of $n = 4$ independent experiments are shown.
- C Western blots of lysates from HCT116 cells transfected with the indicated siRNAs. Where indicated, cells were treated for 6 h with RSPO3 conditioned medium. Representative blots from $n = 3$ independent experiments are shown.
- D TOPflash reporter assays in HCT116 cells upon knockdown of the indicated genes using single siRNAs. Cells were stimulated with control or Wnt3a conditioned medium. Data are displayed as mean \pm SD and show one representative of $n = 3$ independent experiments with three biological replicates.
- E, F qPCR analysis of *USP42*, *LGR5* and *AXIN2* expression levels in HCT116 cells. Data are displayed as mean \pm SD and show $n = 4$ (E) or $n = 3$ (F) independent experiments.

Data information: Statistical significance was calculated by one-way ANOVA analyses with Tukey correction and defined as $**P < 0.01$, $***P < 0.001$, or n.s.: not significant.

different siRNAs (Figs 5E and F, and EV4A; wt HCT116 cells). In line with the requirement of paracrine Wnt signalling for USP42 activity, genetic ablation of Wnt Ligand Secretion Mediator (WLS (Evi)), as well as ectopic expression of ZNRF3, rescued siUSP42 and restored E-cadherin protein levels (Figs 5E and F, and EV4B). Furthermore, as previously shown (Roger *et al*, 2010), knockdown of p53 did not reduce E-cadherin levels in HCT116 cells (Fig EV4C). We next examined HCT116 cells upon genetic ablation of USP42 using CRISPR/Cas9, which resulted in loss of E-cadherin protein levels (Fig 5G and H), thereby phenocopying siUSP42 (Fig 5E and F). We conclude that USP42 prevents EMT in HCT116 cells by inhibiting paracrine Wnt signalling.

Next, we analysed whether USP42 impacts cell survival and clonogenic capacity by performing colony formation experiments. As previously shown (Voloshanenko *et al*, 2013), inhibition of Wnt secretion reduced the colony-forming efficiency of HCT116 cells (Fig EV4D). Conversely, knockdown of USP42 increased colony

formation in HCT116 cells (Fig EV4D and E). As in the case of spheroid growth, treatment with PORCN inhibitors, genetic ablation of WLS (Evi), as well as by ectopic expression of ZNRF3 (Fig EV4D and E) rescued clonogenic capacity induced by USP42 knockdown.

To investigate whether USP42 inhibits Wnt-driven cell proliferation, we performed spheroid assays, which are more representative for the *in vivo* growth conditions than 2D cultures, as they recapitulate tumour cell clusters (Timmins *et al*, 2004). We cultured HCT116 cells in hanging drops for up to 6 days, which resulted in spheroids of ~ 0.3 mm² (Fig 5I and J). Knockdown of USP42 by four independent siRNAs strongly promoted spheroid growth and branching (Figs 5I and J, and EV4F). Importantly, this effect relied on Wnt secretion: First, siUSP42-induced spheroid growth was blocked by the genetic ablation of WLS (Evi) (Fig 5I and J), as well as by the PORCN inhibitors IWP-2 and LGK-974 (Figs 5K and EV4F). Second, ectopic expression of ZNRF3 also rescued spheroid growth upon siUSP42 (Fig EV4G). Furthermore, genetic ablation of

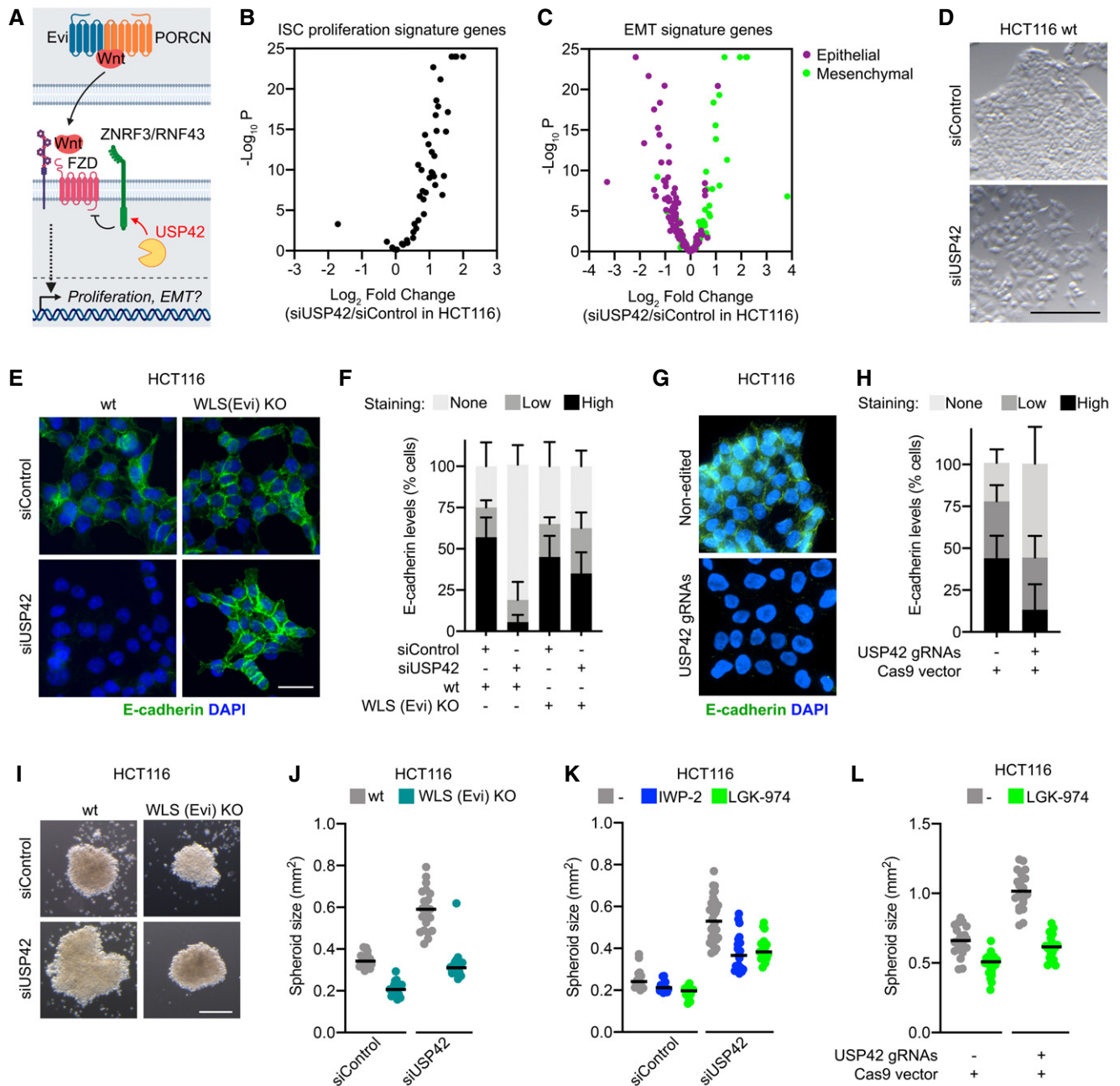


Figure 5. Loss of USP42 leads to Wnt-dependent proliferation and EMT.

A Scheme showing the proposed functions of ZNRF3/RNF43 and USP42 in colorectal cancer cells. Auto- and paracrine Wnt secretion is promoted by Evi (WLS) and PORCN.

B, C Volcano plots representing the genes that conform the Intestinal Stem Cell (ISC) signature (Merlos-Suarez *et al*, 2011) (B, $n = 45$ genes, Dataset EV1F), and the EMT signature in cancer cells (Rokavec *et al*, 2017) (C, $n = 171$ genes, Dataset EV1G) upon USP42 knockdown in HCT116 cells. Significance was capped at $-\log_{10}P = 24$.

D Bright field images of HCT116 cells upon USP42 knockdown. Scale bar = 500 μm .

E, H Immunofluorescence microscopy showing endogenous E-cadherin levels in wt and WLS (Evi) KO HCT116 cells upon transfection with siUSP42 (E), or electroporation with eSpCas9 empty plasmid (non-edited) or eSpCas9-USP42 gRNAs (G). Scale bar = 20 μm . In (F, G), quantification of the fluorescent signal (Alexa-488) in $n \geq 4$ biological replicates with $n \geq 15$ cells per replicate are shown.

I–L Spheroid formation experiments with HCT116 cells upon transfection with siUSP42 (I–K) or electroporation with eSpCas9 empty plasmid (non-edited) or eSpCas9-USP42 gRNAs (L). Scale bar = 500 μm . Where indicated, cells were treated with 5 μM IWP-2 or 20 μM LGK-974 (PORCN inhibitors). The median size was quantified for $n \geq 13$ spheroids from a representative experiment repeated independently $n \geq 3$ is shown.

Data information: Data are displayed as mean \pm SD (F,H) or median (J–L) of the indicated biological replicates and show one representative of $n \geq 3$ independent experiments.

USP42 in HCT116 cells using CRISPR/Cas9 also increased spheroid growth, which was inhibited by LGK-974 (Fig 5K and L).

A role of USP42 in halting Wnt-dependent colorectal cancer cell maintenance was also observed in RKO cells. As in the case of HCT116 cells, knockdown of USP42 in RKO promoted spheroid growth and colony formation, which was blocked by PORCN inhibitors (Fig EV5A–C). Unlike HCT116 cells, RKO cells do not express E-cadherin and already display a mesenchymal phenotype (Hur et al, 2013), independently of USP42 knockdown (Fig EV5D).

Taken together, our data suggest that USP42 functions as a roadblock for proliferation and EMT in colon cancer cells by keeping paracrine Wnt signalling in check (Fig 5A).

USP42 KO mouse organoids survive R-spondin withdrawal

RNF43/ZNRF3 and R-spondin are best known for their roles in intestine homeostasis (Hao et al, 2012; Koo et al, 2012; Koo et al,

2015), which can be examined using organoids. For instance, *Znrf3/Rnf43* double KO mouse small intestinal organoids grow in the absence of R-spondin, fully relying on paracrine Wnt secretion (Koo et al, 2012). We generated *Usp42* KO intestinal organoids by electroporation of a CRISPR-concatemer vector containing two independent *Usp42* gRNAs, followed by positive selection upon RSPO1 withdrawal (Andersson-Rolf et al, 2016; Merenda et al, 2017), see methods). In the presence of exogenous RSPO1 and Wnt surrogates (Janda et al, 2017), both wt and *Usp42* KO organoids grew and formed cyst-like structures (Fig 6A and B), which are caused by the expansion of undifferentiated cells (Mustata et al, 2013; Merenda et al, 2020). Removal of exogenous Wnt led to a swift from cystic to the typical branched structure in the wt organoids (Fig 6A and B) (Koo et al, 2012; Merenda et al, 2017). Consistent with the role of USP42 in RNF43/ZNRF3 regulation, *Usp42* KO organoids still formed cyst-like structures upon exogenous Wnt withdrawal (Fig 6A and B). Importantly, R-spondin withdrawal compromised

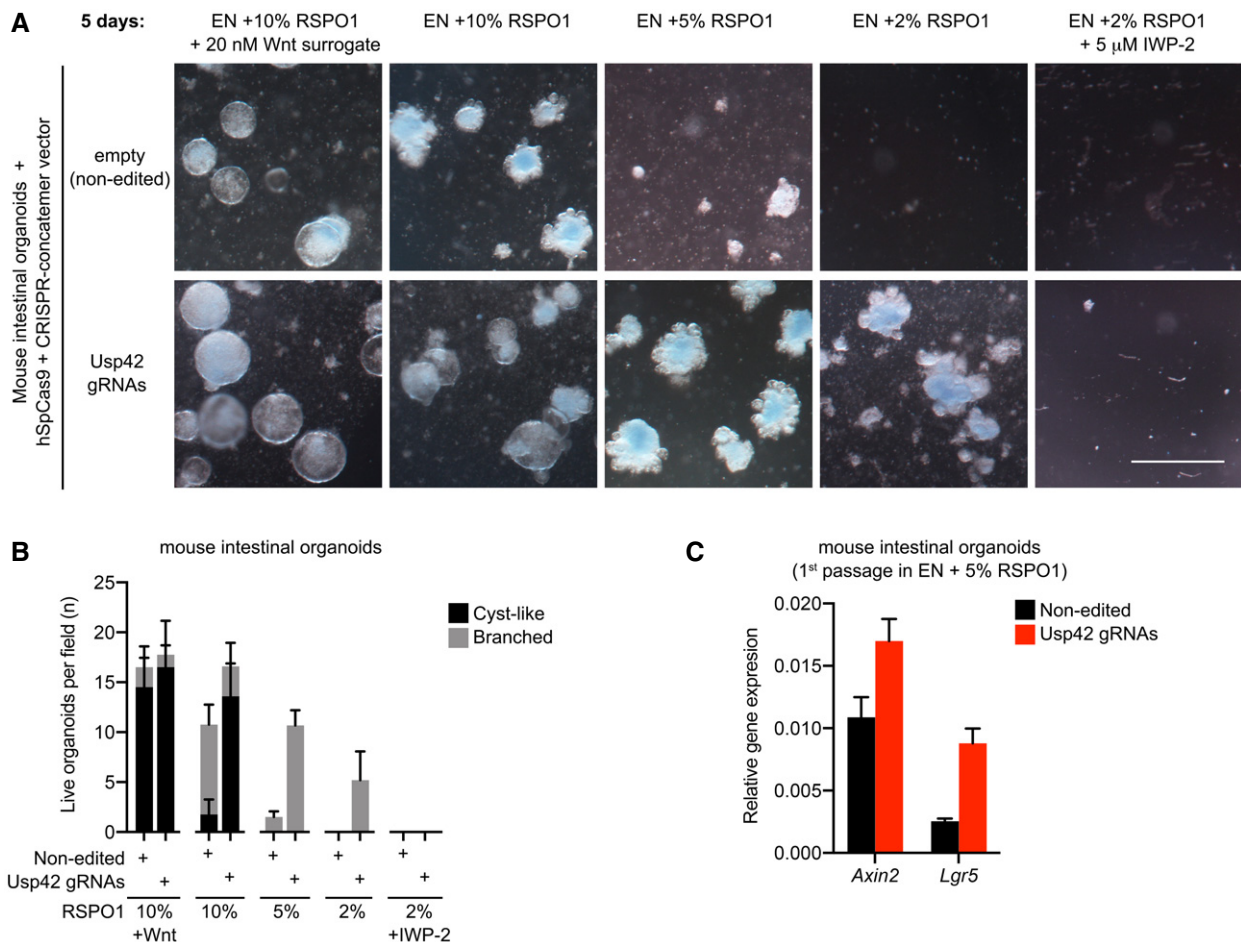


Figure 6. Genetic ablation of *Usp42* renders mouse intestinal organoids Wnt hypersensitive.

A Representative images of mouse small intestinal organoids generated with empty (Non-edited) or USP42gRNA containing CRISPR-concatemers and cultured for 3 days in matrigel with the indicated growth factors, or the Wnt secretion inhibitor IWP-2. EN, EGF and noggin. Note that knockout of *Usp42* (*Usp42* gRNAs) rendered the organoids insensitive to RSPO1 withdrawal. Scale bar = 1 mm.

B Quantification of the number and subtype of organoids from (A).

C qPCR analysis of *Lgr5* and *Axin2* expression levels in first passage mouse intestinal organoids cultured in EN + 5% RSPO1.

Data information: Data are displayed as mean \pm SD of $n \geq 4$ wells and show one representative of $n = 3$ independent experiments.

the viability of wt organoids, but not of the *Usp42* KO organoids (Fig 6A and B), indicating that loss of *Usp42* confers hypersensitivity to paracrine Wnt signalling. Accordingly, i) inhibition of Wnt secretion by IWP-2 led to apoptosis in both *Usp42* KO and wt organoids (Fig 6A and B) and ii) *Usp42* KO organoids displayed higher expression of Wnt target genes *Lgr5* and *Axin2* compared to wt organoids (Fig 6C). Taken together we concluded that *Usp42* inhibits paracrine Wnt signalling in mouse small intestinal organoids.

Discussion

Here, we show that USP42 stabilises ZNRF3 and RNF43 at the plasma membrane. We found that USP42 blocks ubiquitination and clearance of ZNRF3/RNF43 by R-spondin. As a consequence, ZNRF3/RNF43 promote turnover of the Wnt receptors LRP6 and FZD, leading to Wnt signalling inhibition. Furthermore, our study demonstrates that USP42 antagonises Wnt-dependent proliferation, survival and EMT in colon cancer cells and contributes to niche factor dependency in mouse intestinal organoids.

Our data suggest that catalytic activity of USP42 stalls the LGR/ZNRF3 complex at the plasma membrane by preventing RSP0- and ubiquitin-dependent internalisation of ZNRF3. This is also supported by the fact that ZNRF3 Δ Ring, which lacks auto-ubiquitination activity, has a higher residence at the plasma membrane and shows increased interaction with LGR and R-spondin compared to wt ZNRF3 (Hao *et al*, 2012). We also found that USP42 interacts with the Dishevelled interacting region (DIR) of ZNRF3. This supports recent evidence pointing to the relevance of this region in modulating ZNRF3/RNF43 activity. For instance, Dishevelled binding at the DIR is required for ZNRF3/RNF43 function towards the Wnt receptors (Jiang *et al*, 2015). Furthermore, the analysis of tumour relevant truncations in the RNF43 intracellular domain (ICD), including the DIR, identified alternative roles of the β -catenin destruction complex (AXIN1 and CK1 α) in regulating oncogenic RNF43 activity (Spit *et al*, 2020; Tsukiyama *et al*, 2020). CK1 α and β -TrCP have also been proposed to mediate proteasomal degradation of ZNRF3 via a phospho-degron at the DIR (Ci *et al*, 2018). However, it is still unclear whether this function is linked to R-spondin. Finally, PTPRK, which is often fused to RSPO3 in colorectal cancer (Seshagiri *et al*, 2012), has been recently found to dephosphorylate tyrosine residues at the ZNRF3 DIR to promote its internalisation (Chang *et al*, 2020). Future structural data and additional testing might help to resolve how the ZNRF3/RNF43 DIR integrates different signals to control the functions of these E3 ligases (Bugter *et al*, 2020).

ZNRF3 and RNF43 sit at the top of canonical and non-canonical Wnt receptors. As such, it would be interesting to explore whether USP42 also contributes to other Wnt functions including stabilisation of proteins (Wnt/STOP) (Taelman *et al*, 2010; Acebron *et al*, 2014), activation of macropinocytosis (Tejeda-Munoz *et al*, 2019) and modulation of Wnt/Jun and Wnt/Ca⁺² (Tsukiyama *et al*, 2015).

Our results indicate that USP42 provides a barrier against paracrine Wnt signalling in colorectal cancer cells and intestinal organoids. First, we confirmed that paracrine Wnt signalling promotes colorectal cancer cell survival and proliferation (Voloshanenko *et al*, 2013; Koo *et al*, 2015). Second, we found that this paracrine Wnt activity in colon cancer cells was highly underestimated due to a roadblock established by USP42/ZNRF3/RNF43 (Figs 4 and 5).

Third, we identified that paracrine Wnt signalling can promote EMT in colon cancer cells in the absence of USP42 (Fig 5), which further supports a recently proposed role of ZNRF3/RNF43 in blocking EMT (Gujral *et al*, 2014; Hao *et al*, 2016; Wang *et al*, 2016; Murillo-Garzon & Kypta, 2017). Of note, expression of FZD2 is associated with EMT in colorectal cancer cells (Gujral *et al*, 2014), while FZD7 promotes differentiation and mesenchymal-to-epithelial transition (MET) (Vincan *et al*, 2007). Thus, differential Frizzled expression may provide a context-dependent role for paracrine Wnt, RNF43/ZNRF3 and USP42 in EMT. Fourth, we demonstrated that depletion of *Usp42* renders mouse intestinal organoids hypersensitive to secreted Wnt, suggesting that USP42 could play a role in intestine homeostasis, which remains uncharacterised.

USP42 also promotes p53-dependent genotoxic response (Hock *et al*, 2011) (Fig EV2). Together with our data, this highlights USP42 as a potential keystone that sits at the interface between p53 and Wnt signalling. Thus, a standing question is whether USP42 deregulation could bypass the requirement for the sequential misregulation of Wnt and p53 during tumour progression (Vogelstein *et al*, 2013). Interestingly, somatic uncharacterised mutations in USP42 are present in 2–6% of colorectal cancer samples (Cancer Genome Atlas, 2012; Seshagiri *et al*, 2012), reaching up to 11% in the mucinous adenocarcinoma of colon and rectum subtype (Cancer Genome Atlas, 2012), which remain uncharacterised. Furthermore, 23% of squamous cell carcinoma samples harbour uncharacterised mutations in USP42, compared with 28% in APC and 10% in RNF43 (Pickering *et al*, 2014). In addition, USP42 is also recurrently fused to the tumour suppressor RUNX1 in acute myeloid leukaemia (AML) (Paulsson *et al*, 2006; Foster *et al*, 2010; Zagaria *et al*, 2014), which is a tumour fuelled by Wnt signalling (Wang *et al*, 2010). This opens the possibility that not only alterations in RUNX1, but also in USP42, could contribute to AML progression. Our data indicate that USP42 deregulation can be tackled by blocking Wnt secretion with clinically available PORCN inhibitors. Thus, exploring the roles of USP42 in these cancer types could open new avenues for therapeutic intervention.

The functions of USP42 *in vivo* remain largely unknown. To our knowledge, no *Usp42* KO mouse model has been yet characterised. Interestingly, gene trapping of both *Usp42* alleles leads to changes in mouse body size and behaviour, vision impairment, defects in the immune and endocrine systems, and infertility (Adissu *et al*, 2014). However, it remains unclear whether this mouse model is a hypomorph or a null, as well as the molecular mechanisms underlying those phenotypes. Given the wide range of functions of ZNRF3/RNF43 in embryogenesis (Chang *et al*, 2020; Lee *et al*, 2020), limb development (Szenker-Ravi *et al*, 2018), liver zonation (Planas-Paz *et al*, 2016), intestinal tract and adrenal gland homeostasis (Koo *et al*, 2012; Basham *et al*, 2019) and sex determination (Harris *et al*, 2018), it would be important to explore whether USP42 also contributes to these biological functions.

Materials and Methods

Cell culture

HEK293T cells (ATCC) were cultured in DMEM (Gibco), and HCT116 and RKO cells (ATCC) were maintained in RPMI (Gibco)

media supplemented with 1% penicillin/streptomycin and 10% FBS at 37°C and 5% CO₂. Parental and ZNRF3/RNF43 double KO HEK293T cells were kindly provided by M.M. Maurice (Spit *et al*, 2020). The WLS (Evi) KO HCT116 cell line was kindly provided by M. Boutros (Voloshanenko *et al*, 2013). Mouse small intestinal organoids were maintained in growth factor reduced Matrigel (Corning) with IntestiCult Intestinal Organoid Growth Medium (Mouse, Stemcell Technologies) and incubated at 37°C and 5% CO₂. Mycoplasma tests showed that the cell lines were mycoplasma negative.

Wnt3a and control conditioned media were obtained from stably transfected L-cells. R-spondin conditioned media were produced by transiently transfecting HEK293T cells with the indicated R-spondin plasmids (15 µg per 10 cm dish) using calcium phosphate. The media were harvested 24 h after transfection.

Where indicated, cells were treated with 20 nM Bafilomycin A (Sigma), 10 µM MG132 (Sigma), 20 µM LGK-974 (as tested in (Liu *et al*, 2013)), or 5 µM IWP2.

Small interfering RNA (siRNA)

Scrambled (siControl) and siRNAs against human LRP5, LRP6, USP42 #1 (CAGUCUACCUCGAACGCAU), TP53, and APC were obtained from SIGMA. USP42 siRNA #2–4 are single siRNAs from sets of four from Dharmacon. USP42 siRNAs were validated by qPCR and immunofluorescence. HEK293T cells were transfected with 50 nM siRNA using Dharmafect1 transfection reagent (Horizon Discovery) following the manufacturer guidelines. HCT116 cells were transfected with 75 nM siRNA using RNAiMAX (Thermo Fisher) according to the supplier's protocol.

Expression constructs/plasmids

pEGFP-FLAG-USP42 wt and pEGFP-FLAG-USP42^{C120A} plasmids were a kind gift from K.H. Vousden (Hock *et al*, 2011). Wnt1, hLRP6, mFzd8, xDvl-GFP, Dvl1, xβ-catenin, ZNRF3-HA, V5-hLGR4, hRSPO1-ΔC-AP (RSPO1), hRSPO2-ΔC-AP (RSPO2), hRSPO3-ΔC-AP (RSPO3), mRSPO4-AP (RSPO4), TOPflash and Renilla plasmids were kindly provided by C. Niehrs and were described previously (Glinka

et al, 2011; Berger *et al*, 2017; Chang *et al*, 2020). The two gRNA CRISPR-concatemer, RNF43-FLAG-HA and FZD8-V5 plasmids were kind gifts from B.K. Koo and M. Boutros, respectively (Koo *et al*, 2012; Merenda *et al*, 2017; Voloshanenko *et al*, 2017). The V5- and SNAP-FZD5 plasmids were kindly provided by M.M. Maurice. FLAG-HA-USP39 (#22581), 3xFLAG-DVL2 (#24802) and PG13-luc (#16442), hSpCas9 (#42230), eSpCas9-ATP1A1-dual-gRNA (#86613) plasmids were obtained from Addgene. Truncation mutants were generated by PCR: USP42ΔN (N-terminal, Δ1–111), USP42ΔC (C-terminal Δ412–1315), USP42ΔNLS (Predicted nuclear localisation signal, Δ1160–1246), ZNRF3ΔRING (Δ293–334), ZNRF3Δlinker (Δ335–345) and ZNRF3ΔDIR (Δ346–528). The GFP-USP42 and RNF43-FLAG plasmids for the ubiquitination experiments were generated by PCR by removing the FLAG and HA tag from the pEGFP-FLAG-USP42 (Hock *et al*, 2011) and RNF43-FLAG-HA plasmids, respectively (Tables 1 and 2).

CRISPR/Cas9 genome editing

USP42 KO HEK293T and HCT116 cells were created using CRISPR/Cas9 followed by co-selection strategy with ATP1A1, as previously described (Agudelo *et al*, 2017). Briefly, 3 days after the electroporation of the guide RNA (gRNA) and eSpCas9 containing plasmid together with the ATP1A1 template, cells were treated with 0.5 µM of ouabain for 6 days. Parental and USP42 KO HEK293T single clones were picked from the surviving colonies, grown individually and proved for the lack of USP42 protein expression by immunofluorescence (See Fig EV1B). Edited HCT116 cells were used in bulk for the phenotypic experiments in Fig 5 to avoid possible clonal artefacts arisen during the selection of cancer cells.

The Usp42 KO organoids were generated as described previously (Merenda *et al*, 2017). Briefly, mouse intestinal organoids were electroporated with hSpCas9 and a CRISPR-concatemer vector containing two sgRNAs against Usp42 (Table 3) or empty (Non-edited). Electroporated organoids were expanded for 20 days. Organoids electroporated with USP42 gRNAs were subjected to RSPO1 withdrawal for selection, as previously done for other negative regulators of the Wnt pathway (Merenda *et al*, 2017).

Table 1. ZNRF3 truncation mutants were generated with the following primers

Construct	Forward primer	Reverse primer	Tm [°C]
ΔC-terminal	TAAGATATCCAGCACAGTGGCGG	GATTTTGACAAGGAGGATGAGGCAG	69
ΔRING domain	CACAACATCATAGAACAAAAGGAAACC	GTCGGACGTGGAGCTGCTGCT	67
Δlinker	GCGGTGTGTGTGGAGACC	CCGACAGTGGGGCAGGTGT	70
ΔDIR	TTCAGTCTGATCACGGCCACC	GCTTGGTTCCTTTTGTCTATGATGT	70

Table 2. USP42 truncation mutants were generated using the following primers

Construct	Forward primer	Reverse primer	Tm [°C]
ΔN-terminal	CAATACCTGTTTTGCCAATGCAG	CTTATCGTCGTCATCCTTGAATCCAT	65
ΔNLS	TGACTCGAGATCCACCGGAT (same as ΔC)	TCCATTTTCGTGTCGTGAA	63
ΔC-terminal	TGACTCGAGATCCACCGGAT	GGACCTGATATAAAGAGCACAT	63

Table 3. gRNAs used in this study

gRNA		Sequence 5' – 3'
hUSP42#1	Top	CACCGAATCAGCCTGGCAGCTCCG
	Bottom	AAACCGGAGCTGCCAGGCTGATTC
hUSP42#2	Top	CACCGATGCAGTTCGCCAGCTG
	Bottom	AAACCGCTGGCAGAACCTGCATC
mUsp42#1	Top	CACCGGGACACAGGCTCTGCCAGCTGGT
	Bottom	TAAACCGCTGGCAGAGCCTGTGTCCC
mUsp42#2	Top	ACCGGGAGACCGCTCACAACTGCCG
	Bottom	AAAACGGCAGTTGTGAGGCGGTCTCC

Antibodies

The following antibodies were used: mouse anti-alpha-Tubulin (T9026), mouse anti-FLAG M2 (F1804), rabbit anti-USP42 (HPA006752, IF), mouse anti-HA (H3663), rat anti-HA 3F10 (118674230010), chicken anti-GFP from Sigma; mouse anti- β -catenin (610153) and conjugated anti-BrdU-FITC from BD Biosciences; rabbit anti-AXIN (345900, Thermo Fisher); rabbit anti-LRP6 C5C7 (2560S) and rabbit anti-GSK3 β (D5C5Z) from Cell Signaling; rabbit anti-GFP (ab290) and rabbit anti-E-cadherin (ab40772) from Abcam; mouse conjugated anti-LRP6-APC (FAV1505A, R&D Systems); mouse anti-V5 (R960-25, Invitrogen); mouse anti-CD147 8D6 (Santa Cruz sc-21746).

Reporter assays

For the Wnt reporter (TOPflash) assays, HEK293T or HCT116 cells were seeded on a 96-well plate and transfected with 50 ng DNA per well, including 5 ng Firefly luciferase and 3 ng Renilla luciferase, filled up with empty vector (pCS2+). The transfection was performed using X-tremeGENE nine transfection reagent (Roche) following the supplier's protocol. For epistasis experiments, cells were co-transfected with 5 ng GFP-USP42, 5 ng USP39, 0.5 ng ZNRF3-HA, 1 ng RNF43-FLAG-HA, 3 ng hLRP6, 5 ng Wnt1, 1 ng mFzd8, 20 ng Dvl1 or 1 ng χ -catenin. Where indicated, siRNA-mediated knockdown of the indicated genes was performed 24 h prior to DNA transfection. Cells were stimulated for 24 h with control (1:5) or Wnt3a (1:5) conditioned media, with or without R-spondin3- Δ C (1:50) conditioned medium. For p53 reporter assays, HCT116 cells were seeded on a 96-well plate and transfected with 50 ng DNA per well, including 10 ng PG13-luc, 5 ng Renilla and filled with empty vector (pCS2+) using X-tremeGene-9 transfection reagent (Roche) following the supplier's protocol.

Western Blots

Cells were harvested in PBS and lysed in lysis buffer (PBS supplemented with 2% NP-40, 2 mM EDTA, 10 mM β -mercaptoethanol, Proteinase inhibitors (Roche)). Cleared lysates were mixed with either NuPAGE or Laemmli buffer under reducing conditions, and analysed by SDS-PAGE or NuPAGE Bis-Tris gel electrophoresis, followed by Western blotting.

For co-immunoprecipitation experiments, cells seeded in 6-well plates and transfected with 300 ng per well of the indicated

constructs. 24–48 h after transfection, cells were harvested in PBS and three wells were combined per IP. Cells were lysed in co-IP lysis buffer (20 mM Tris-HCl pH 7.5, 150 mM NaCl, 1% Triton X-100 and 1 mM EDTA supplemented with phosphatase protease inhibitors (Roche)) for 10 min on ice. The proteins were immunoprecipitated by incubating the cleared lysates using the indicated antibodies in co-IP lysis buffer and protein A/G agarose (Merck Millipore). Samples were eluted in 2 \times Laemmli or NUPAGE buffer and analysed as indicated above.

For the ubiquitination experiments (Fig 1G and H), cells were grown in 6-well plates. Per IP, four wells were transfected with 5 μ g ZNRF3-FLAG, 5 μ g GFP-USP42 and 2 μ g HA-Ubiquitin wt using calcium phosphate. The medium was changed 5–7 h after transfection. Cells were treated with Bafilomycin A and MG132 for 6 h and harvested 24 h after transfection. Cells were lysed for 10 min on ice in 150 mM NaCl, 1% Triton X-100, 1 mM EDTA and 50 mM Tris-HCl pH 7.5 lysis buffer. Cleared lysates were supplemented with 1% SDS and boiled for 10 min at 95 °C. After reaching room temperature, lysates were diluted 10-times to quench the SDS, and proteins were precipitated by rabbit anti-FLAG antibodies and protein A agarose, eluted in 2 \times NUPAGE buffer and analysed by SDS-PAGE and Western blots.

Expression and mutation data analysis

Gene alterations in colorectal adenocarcinoma from TCGA (Cancer Genome Atlas, 2012) for Fig 4 ($n = 524$) were retrieved from the cBioPortal in 2017 and updated as displayed in 03/2020. Differences between adjacent healthy tissue and tumour samples are shown. We analysed and displayed all available alterations which included copy-number variations, mutations and aberrant mRNA expression with the suggested Z-score threshold ± 2 .

Flow cytometry

For FACS analyses of surface LRP6, HCT116 cells were plated on 6-well plates, transfected with siRNA after 24 h and treated with RSPO3 conditioned medium for 12 h. Cells were harvested in Hank's buffer (HBSS) supplemented with 1 mM EDTA. After centrifugation, cells were resuspended in 200 μ l of 1% BSA in PBS supplemented with 0.1% sodium azide and incubated for 30 min at 4°C, followed by a 4 h incubation with anti-LRP6-APC conjugated antibody. After washing, cells were resuspended in blocking solution containing DAPI and transferred to FACS tubes.

For the BrdU experiments, siRNA transfected HCT116 cells were incubated with 10 μ M BrdU for 6 h before harvesting. Cells were fixed by resuspending the pellet in 70% cold ethanol. Subsequently, cells were treated with 2N HCl including 0.5% Triton X-100 and incubated 30 min at room temperature. Following centrifugation, cells were resuspended in 0.1 M sodium borate pH 8 for 2 min to counter the pH. Cells were washed twice with 2% horse serum in PBS, resuspended in staining solution (PBS, 2% horse serum, 0.5% Tween, anti-BrdU-FITC conjugated antibody) and incubated for 2 h. Finally, cells were centrifuged, resuspended in PBS containing 10 μ g/ml RNase A and 5 μ g/ml propidium iodide (PI) and incubated 30 min in the dark. The fluorescence was analysed in the FACS sorter Canto II (BD Biosciences). Where indicated, cells were synchronised with a double-thymidine block using 500 μ M

thymidine (Acebron *et al*, 2014). During the second thymidine block, cells were co-treated with BrdU for 6 h before harvesting.

Clonogenicity assays

HCT116 cells were plated and transfected with siRNA the next day. 24 h after transfection, HCT116 cells were trypsinised, counted and seeded in 6-well plates (200 cells/well). After one week, cells were washed twice with cold PBS and fixed/stained using a solution of 75% H₂O, 24% methanol and 1% crystal violet for 5 min at room temperature. Wells were washed five times with PBS and dried at room temperature. Pictures were taken with a Nikon SMZ25 microscope.

Surface biotinylation

Cells were seeded on 15-cm plates and transfected at 60% confluency with ZNRF3-FLAG or RNF43-FLAG, HA-Ubiquitin and GFP-USP42 plasmids using CaCl₂ transfection reagent. Surface proteins were biotinylated with EZ-Link Sulfo-NHS-SS-Biotin at 4°C for 30 min. following manufacturer's instructions (Pierce Cell Surface Protein Isolation Kit Cat. Nr. 89881, Thermo Scientific) and pulled down with Neutravidin beads. Cell surface proteins were eluted with Strep-Tactin® Elution Buffer (IBA Lifesciences Cat. Nr. 2-1206-002), diluted up to 1 ml of immunoprecipitation buffer (20 mM Tris-HCl pH 7.5; 150 mM NaCl; 1% Triton X-100, and 1 mM EDTA) and FLAG-tagged ZNRF3/RNF43 were immunoprecipitated with M2 affinity gel (SIGMA, Cat. Nr. A2220). Proteins were eluted with Laemmli buffer under reducing conditions and analysed by SDS-PAGE followed by Western blotting.

Imaging experiments

For USP42 expression experiments, HEK293T cells were seeded on coverslips in 12-well plates. The following day, 125 ng per well of either pEGFP-FLAG-USP42 wt, C120A, ΔN, ΔNLS or ΔC plasmid was transfected using X-tremeGENE nine transfection reagent. Cells were harvested 24 h after transfection, fixed in 2% paraformaldehyde in PBS and stained with DAPI.

Endogenous USP42 was analysed in HEK293T cells transfected with either scrambled siRNA or siRNA against USP42 using DharmaFECT1. 48 h after transfection, cells were fixed in 2% paraformaldehyde in PBS. Cells were stained with rabbit anti-USP42 and anti-rabbit AF488 supplemented with DAPI.

For SNAP labelling, HEK293T cells were seeded on Poly-Lysine coated coverslips in 12-well plates and transfected with 200 ng empty vector, 100 ng SNAP-tagged Frizzled, 100 ng GFP-USP42 and 100 ng of ZNRF3-HA plasmids. 24 h after transfection, cells were incubated in 1 μM SNAP-Surface 549 reagent (NEB) for 15 min at room temperature in the dark as previously described (Koo *et al*, 2012). Cells were washed twice, chased for 10 min and fixed with 4% paraformaldehyde in PBS. Coverslips were imaged with the Eclipse T_i with NIS Elements using a 60× magnification objective with oil immersion.

For HCT116 and RKO spheroids, 2,000 cells were seeded one day after siRNA transfection in 30 μL hanging drops containing RPMI (Gibco), supplemented with 5% FBS. Treatments were applied during seeding as indicated. Spheroid growth was measured 6 days

after seeding using a Nikon SMZ25 microscope. Afterwards, single spheroid area was measured with Fiji.

For the organoid imaging experiments, mouse intestinal organoids edited with hSpCas9 as indicated above, were culture as previously described (Merenda *et al*, 2017). Briefly, organoids were seeded in matrigel and grown for 5 days in basal medium containing 50 ng/mL mouse EGF and 100 ng/mL mouse Noggin together with i) 20 nM Wnt surrogates (Janda *et al*, 2017) and 10% RSPO1 conditioned medium (CM), ii) 10% RSPO1 CM, iii) 5% RSPO1 CM, iv) 2% RSPO1 CM or v) 2% RSPO1 CM supplemented with 5 μM IWP-2. The organoids were imaged in a Nikon SMZ25 microscope.

Real-time PCR

RNA was extracted by using the RNeasy Mini Kit (QIAGEN). The cDNA was synthesised from 1 μg of total RNA by using the Bioline SensiFAST cDNA Synthesis Kit. Quantitative PCR was performed with the SensiFAST SYBR Hi-ROX Kit (Bioline) using a StepOnePlus 96-well plate reader (Applied Biosystems). For RT-PCR data analysis, normalisation of gene expression was carried out to the house-keeping gene *GAPDH* (human) or *Gapdh* (mouse). Where indicated, cells were harvested 48 h after siRNA transfection.

RNA-sequencing preparation and analysis

HCT116 cells were seeded in 6-well plates, transfected with siRNA 24 h later and harvested 48 h after transfection ($N = 3$ biological independent experiments). RNA was extracted by using the RNeasy Mini Kit (QIAGEN). RNA integrity (RIN value) of all samples was assessed in an Agilent 2100 Bioanalyzer machine using an Agilent RNA 6000 Nano chip. After, library preparation of the RNA samples was performed using a NEBNext Ultra II RNA Library Prep Kit for Illumina. cDNA library quality and concentration were measured in an Agilent 2100 Bioanalyzer machine using an Agilent High Sensitivity DNA chip. After, libraries from all barcoded samples were pooled and sequenced. Sequencing reads were quality controlled using FastQC (<http://www.bioinformatics.s.babraham.ac.uk/projects/fastqc/>) tool (version 0.11.5). Read alignments, as well as count tables of mapped read per gene, were obtained by using STAR version 2.6.0a (Dobin *et al*, 2013) with GRCh38 human reference genome and its gene model (GRCh38.84). The dataset was uploaded to ENA with the accession number PRJEB37946.

Differentially expressed genes were identified with DESeq2 version 2.1.20 (Anders & Huber, 2010) in R (See Dataset EV1A,B). The significant up- and downregulated genes (FDR < 0.1) were used for pathway and gene ontology (GO) (The Gene Ontology Consortium, 2019) enrichment analysis using the MGSA package (Bauer *et al*, 2010) (see Dataset EV1C,D). In order to create the Functional Annotated Clustering of the GO terms, we selected the ID of the top 3,000 differentially upregulated genes from the Dataset EV1A and generated a list in DAVID Bioinformatics Database (da Huang *et al*, 2009). We selected Gene_Ontology_BP_direct database and combined view for selected annotation. The results appear in Dataset EV1E. Gene Set Enrichment Analysis plots (Fig EV3) were generated using the R package fgsea (version 1.6.0, Sergushichev, bioRxiv <https://doi.org/10.1101/060012>) with hallmark gene sets (human_H_v5p2) and GO gene sets (human_c5_v5p2).

Image data processing

Raw images were imported to Fiji (ImageJ, v2.0) prior to their export to Photoshop 2020 for figure arrangement. Linear changes in contrast or brightness were equally applied to all controls and across the entire images. The models and schemes were created with Biorender.com.

Statistical analyses

Data are shown as mean with standard error of the mean (SEM or SD), as indicated in the figure legends; except for Figs 5J–L, EV4F and G, and EV5B where median values are represented. Where indicated, Student's *t*-tests (two groups) or one-way ANOVA analyses with Tukey correction (three or more groups) were calculated using Prism v8. Significance is indicated as: **P* < 0.05, ***P* < 0.01, ****P* < 0.001, or n.s.: not significant.

Data availability

RNA-seq data generated in this study is available on the European Nucleotide Archive (ENA) with the accession number PRJEB37946 (<https://www.ebi.ac.uk/ena/browser/view/PRJEB37946>).

Expanded View for this article is available online.

Acknowledgements

We thank M. Boutros, C. Niehrs, M.M. Maurice, B.K. Koo, G. Pereira, T.W. Holstein, S. Özbek, H. Bastians, C.Y. Janda, K.C. Garcia and K.H. Voudsen for sharing reagents. We thank A. Ciprianidis, the Nikon Imaging Facility (Heidelberg University), the Genomics Core Facility (EMBL) and the FACS core facility (Heidelberg University) for technical help. VF-S and MT are research collaborators (Technical University of Munich). We thank H. Bastians, T. Holstein and M. Boutros for critical reading of the manuscript. This work was supported by the Deutsche Forschungsgemeinschaft (DFG) through the research grant PE 2674/1 (SPA and NG), the SFB1324 (SPA and AGA) and SFB1335 (Project number 360372040) (VF-S). AJS holds a Humboldt Research Fellowship for Postdoctoral Researchers. Open Access funding enabled and organized by ProjektDEAL.

Author contributions

NG, AJS and SPA conceived, performed and analysed experiments. AJS, JJML, LV and VB performed and analysed the RNA-seq experiment. VF-S and MT performed the surface biotinylation experiments. AGA generated the USP42 constructs and assisted on experiments. SPA supervised all aspects of the project. SPA, AJS and NG wrote the manuscript with input from all authors.

Conflict of interest

The authors declare that they have no conflict of interest.

References

- Acebron SP, Karaulanov E, Berger BS, Huang YL, Niehrs C (2014) Mitotic wnt signaling promotes protein stabilization and regulates cell size. *Mol Cell* 54: 663–674
- Adissu HA, Estabel J, Sunter D, Tuck E, Hooks Y, Carragher DM, Clarke K, Karp NA, Sanger Mouse Genetics P, Newbigging S et al (2014) Histopathology reveals correlative and unique phenotypes in a high-throughput mouse phenotyping screen. *Dis Model Mech* 7: 515–524
- Agudelo D, Durringer A, Bozoyan L, Huard CC, Carter S, Loefer J, Synodinou D, Drouin M, Salsman J, Delliare G et al (2017) Marker-free coselection for CRISPR-driven genome editing in human cells. *Nat Methods* 14: 615–620
- Anders S, Huber W (2010) Differential expression analysis for sequence count data. *Genome Biol* 11: R106
- Andersson-Rolf A, Merenda A, Mustata RC, Li T, Dietmann S, Koo BK (2016) Simultaneous paralogue knockout using a CRISPR-concatemer in mouse small intestinal organoids. *Dev Biol* 420: 271–277
- Basham KJ, Rodriguez S, Turcu AF, Lerario AM, Logan CY, Rysztak MR, Gomez-Sanchez CE, Breault DT, Koo BK, Clevers H et al (2019) A ZNRF3-dependent Wnt/beta-catenin signaling gradient is required for adrenal homeostasis. *Genes Dev* 33: 209–220
- Bauer S, Gagneur J, Robinson PN (2010) GOing Bayesian: model-based gene set analysis of genome-scale data. *Nucleic Acids Res* 38: 3523–3532
- Berger BS, Acebron SP, Herbst J, Koch S, Niehrs C (2017) Parkinson's disease-associated receptor GPR37 is an ER chaperone for LRP6. *EMBO Rep* 18: 712–725
- Bilic J, Huang YL, Davidson G, Zimmermann T, Cruciat CM, Bienz M, Niehrs C (2007) Wnt induces LRP6 signalosomes and promotes dishevelled-dependent LRP6 phosphorylation. *Science* 316: 1619–1622
- Bond CE, McKeone DM, Kalimutho M, Bettington ML, Pearson SA, Dumenil TD, Wockner LF, Burge M, Leggett BA, Whitehall VL (2016) RNF43 and ZNRF3 are commonly altered in serrated pathway colorectal tumorigenesis. *Oncotarget* 7: 70589–70600
- Bugter JM, Fenderico N, Maurice MM (2020) Mutations and mechanisms of WNT pathway tumour suppressors in cancer. *Nat Rev Cancer* 21: 5–21
- Cancer Genome Atlas N (2012) Comprehensive molecular characterization of human colon and rectal cancer. *Nature* 487: 330–337
- Cano A, Perez-Moreno MA, Rodrigo I, Locascio A, Blanco MJ, del Barrio MG, Portillo F, Nieto MA (2000) The transcription factor snail controls epithelial-mesenchymal transitions by repressing E-cadherin expression. *Nat Cell Biol* 2: 76–83
- Carmon KS, Gong X, Lin Q, Thomas A, Liu Q (2011) R-spondins function as ligands of the orphan receptors LGR4 and LGR5 to regulate Wnt/beta-catenin signaling. *Proc Natl Acad Sci USA* 108: 11452–11457
- Chang LS, Kim M, Glinka A, Reinhard C, Niehrs C (2020) The tumor suppressor PTPRK promotes ZNRF3 internalization and is required for Wnt inhibition in the Spemann organizer. *eLife* 9: e51248
- Ci Y, Li X, Chen M, Zhong J, North BJ, Inuzuka H, He X, Li Y, Guo J, Dai X (2018) SCF(beta-TRCP) E3 ubiquitin ligase targets the tumor suppressor ZNRF3 for ubiquitination and degradation. *Protein Cell* 9: 879–889
- Clevers H, Loh KM, Nusse R (2014) Stem cell signaling. An integral program for tissue renewal and regeneration: Wnt signaling and stem cell control. *Science* 346: 1248012
- Dobin A, Davis CA, Schlesinger F, Drenkow J, Zaleski C, Jha S, Batut P, Chaisson M, Gingeras TR (2013) STAR: ultrafast universal RNA-seq aligner. *Bioinformatics* 29: 15–21
- Fenderico N, van Scherpenzeel RC, Goldflam M, Proverbio D, Jordens I, Kralj T, Stryeck S, Bass TZ, Hermans G, Ullman C et al (2019) Anti-LRP5/6 VHHs promote differentiation of Wnt-hypersensitive intestinal stem cells. *Nat Commun* 10: 365
- Foster N, Paulsson K, Sales M, Cunningham J, Groves M, O'Connor N, Begum S, Stubbs T, McMullan DJ, Griffiths M et al (2010) Molecular characterisation of a recurrent, semi-cryptic RUNX1 translocation t(7;21) in myelodysplastic syndrome and acute myeloid leukaemia. *Br J Haematol* 148: 938–943

- Frailie JM, Quesada V, Rodriguez D, Freije JM, Lopez-Otin C (2012) Deubiquitinases in cancer: new functions and therapeutic options. *Oncogene* 31: 2373–2388
- Giannakis M, Hodis E, Jasmine MuX, Yamauchi M, Rosenbluh J, Cibulskis K, Saksena G, Lawrence MS, Qian ZR, Nishihara R et al (2014) RNF43 is frequently mutated in colorectal and endometrial cancers. *Nat Genet* 46: 1264–1266
- Glinka A, Dolde C, Kirsch N, Huang YL, Kazanskaya O, Ingelfinger D, Boutros M, Cruciat CM, Niehrs C (2011) LGR4 and LGR5 are R-spondin receptors mediating Wnt/beta-catenin and Wnt/PCP signalling. *EMBO Rep* 12: 1055–1061
- Gujral TS, Chan M, Peshkin L, Sorger PK, Kirschner MW, MacBeath G (2014) A noncanonical Frizzled2 pathway regulates epithelial-mesenchymal transition and metastasis. *Cell* 159: 844–856
- Han T, Schatoff EM, Murphy C, Zafra MP, Wilkinson JE, Elemento O, Dow LE (2017) R-Spondin chromosome rearrangements drive Wnt-dependent tumour initiation and maintenance in the intestine. *Nat Commun* 8: 15945
- Hao HX, Jiang X, Cong F (2016) Control of Wnt Receptor Turnover by R-spondin-ZNRF3/RNF43 Signaling Module and Its Dysregulation in Cancer. *Cancers (Basel)* 8: 54
- Hao HX, Xie Y, Zhang Y, Charlat O, Oster E, Avello M, Lei H, Mickanin C, Liu D, Ruffner H et al (2012) ZNRF3 promotes Wnt receptor turnover in an R-spondin-sensitive manner. *Nature* 485: 195–200
- Harris A, Siggers P, Corrochano S, Warr N, Sagar D, Grimes DT, Suzuki M, Burdine RD, Cong F, Koo BK et al (2018) ZNRF3 functions in mammalian sex determination by inhibiting canonical WNT signaling. *Proc Natl Acad Sci USA* 115: 5474–5479
- Hock AK, Vigneron AM, Carter S, Ludwig RL, Vousden KH (2011) Regulation of p53 stability and function by the deubiquitinating enzyme USP42. *EMBO J* 30: 4921–4930
- Hock AK, Vigneron AM, Vousden KH (2014) Ubiquitin-specific peptidase 42 (USP42) functions to deubiquitylate histones and regulate transcriptional activity. *J Biol Chem* 289: 34862–34870
- da Huang W, Sherman BT, Lempicki RA (2009) Systematic and integrative analysis of large gene lists using DAVID bioinformatics resources. *Nat Protoc* 4: 44–57
- Hur K, Toiyama Y, Takahashi M, Balaguer F, Nagasaka T, Koike J, Hemmi H, Koi M, Boland CR, Goel A (2013) MicroRNA-200c modulates epithelial-to-mesenchymal transition (EMT) in human colorectal cancer metastasis. *Gut* 62: 1315–1326
- Janda CY, Dang LT, You C, Chang J, de Lau W, Zhong ZA, Yan KS, Marecic O, Siepe D, Li X et al (2017) Surrogate Wnt agonists that phenocopy canonical Wnt and beta-catenin signalling. *Nature* 545: 234–237
- Jiang X, Charlat O, Zamponi R, Yang Y, Cong F (2015) Dishevelled promotes Wnt receptor degradation through recruitment of ZNRF3/RNF43 E3 ubiquitin ligases. *Mol Cell* 58: 522–533
- Jiang X, Hao HX, Growney JD, Woolfenden S, Bottiglio C, Ng N, Lu B, Hsieh MH, Bagdasarian L, Meyer R et al (2013) Inactivating mutations of RNF43 confer Wnt dependency in pancreatic ductal adenocarcinoma. *Proc Natl Acad Sci USA* 110: 12649–12654
- Jung YS, Park JI (2020) Wnt signaling in cancer: therapeutic targeting of Wnt signaling beyond beta-catenin and the destruction complex. *Exp Mol Med* 52: 183–191
- Kazanskaya O, Glinka A, Barrantes ID, Stannek P, Niehrs C, Wu W (2004) R-spondin2 is a secreted activator of Wnt/beta-catenin signaling and is required for Xenopus myogenesis. *Dev Cell* 7: 525–534
- Kazanskaya O, Ohkawara B, Heroult M, Wu W, Maltry N, Augustin HG, Niehrs C (2008) The Wnt signaling regulator R-spondin 3 promotes angioblast and vascular development. *Development* 135: 3655–3664
- Koo BK, van Es JH, van den Born M, Clevers H (2015) Porcupine inhibitor suppresses paracrine Wnt-driven growth of Rnf43;Znrf3-mutant neoplasia. *Proc Natl Acad Sci USA* 112: 7548–7550
- Koo BK, Spit M, Jordens I, Low TY, Stange DE, van de Wetering M, van Es JH, Mohammed S, Heck AJ, Maurice MM et al (2012) Tumour suppressor RNF43 is a stem-cell E3 ligase that induces endocytosis of Wnt receptors. *Nature* 488: 665–669
- de Lau W, Barker N, Low TY, Koo BK, Li VS, Teunissen H, Kujala P, Haegebarth A, Peters PJ, van de Wetering M et al (2011) Lgr5 homologues associate with Wnt receptors and mediate R-spondin signalling. *Nature* 476: 293–297
- de Lau W, Peng WC, Gros P, Clevers H (2014) The R-spondin/Lgr5/Rnf43 module: regulator of Wnt signal strength. *Genes Dev* 28: 305–316
- Lee H, Seidl C, Sun R, Glinka A, Niehrs C (2020) R-spondins are BMP receptor antagonists in Xenopus early embryonic development. *Nat Commun* 11: 5570
- Leung C, Tan SH, Barker N (2018) Recent Advances in Lgr5(+) Stem Cell Research. *Trends Cell Biol* 28: 380–391
- Liu J, Pan S, Hsieh MH, Ng N, Sun F, Wang T, Kasibhatla S, Schuller AG, Li AG, Cheng D et al (2013) Targeting Wnt-driven cancer through the inhibition of Porcupine by LGK974. *Proc Natl Acad Sci USA* 110: 20224–20229
- MacGurn JA, Hsu PC, Emr SD (2012) Ubiquitin and membrane protein turnover: from cradle to grave. *Annu Rev Biochem* 81: 231–259
- Merenda A, Andersson-Rolf A, Mustata RC, Li T, Kim H, Koo BK (2017) A Protocol for Multiple Gene Knockout in Mouse Small Intestinal Organoids Using a CRISPR-concatemer. *J Vis Exp* 125: e55916
- Merenda A, Fenderico N, Maurice MM (2020) Wnt signaling in 3D: recent advances in the applications of intestinal organoids. *Trends Cell Biol* 30: 60–73
- Merlos-Suarez A, Barriga FM, Jung P, Iglesias M, Cespedes MV, Rossell D, Sevillano M, Hernando-Momblona X, da Silva-Diz V, Munoz P et al (2011) The intestinal stem cell signature identifies colorectal cancer stem cells and predicts disease relapse. *Cell Stem Cell* 8: 511–524
- Murillo-Garzon V, Kypta R (2017) WNT signalling in prostate cancer. *Nat Rev Urol* 14: 683–696
- Mustata RC, Vasile G, Fernandez-Vallone V, Strollo S, Lefort A, Libert F, Monteyne D, Perez-Morga D, Vassart G, Garcia MI (2013) Identification of Lgr5-independent spheroid-generating progenitors of the mouse fetal intestinal epithelium. *Cell Rep* 5: 421–432
- Niehrs C (2010) On growth and form: a Cartesian coordinate system of Wnt and BMP signaling specifies bilaterian body axes. *Development* 137: 845–857
- Nieto MA, Huang RY, Jackson RA, Thiery JP (2016) EMT: 2016. *Cell* 166: 21–45
- Nusse R, Clevers H (2017) Wnt/beta-catenin signaling, disease, and emerging therapeutic modalities. *Cell* 169: 985–999
- Paulsson K, Bekassy AN, Olofsson T, Mitelman F, Johansson B, Panagopoulos I (2006) A novel and cytogenetically cryptic t(7;21)(p22;q22) in acute myeloid leukemia results in fusion of RUNX1 with the ubiquitin-specific protease gene USP42. *Leukemia* 20: 224–229
- Pickering CR, Zhou JH, Lee JJ, Drummond JA, Peng SA, Saade RE, Tsai KY, Curry JL, Tetzlaff MT, Lai SY et al (2014) Mutational landscape of aggressive cutaneous squamous cell carcinoma. *Clin Cancer Res* 20: 6582–6592
- Planas-Paz L, Orsini V, Boulter L, Calabrese D, Pikiolek M, Nigsch F, Xie Y, Roma G, Donovan A, Marti P et al (2016) The RSPO-LGR4/5-ZNRF3/RNF43 module controls liver zonation and size. *Nat Cell Biol* 18: 467–479
- Roger L, Jullien L, Gire V, Roux P (2010) Gain of oncogenic function of p53 mutants regulates E-cadherin expression coupled from cell invasion in colon cancer cells. *J Cell Sci* 123: 1295–1305

- Rokavec M, Kaller M, Horst D, Hermeking H (2017) Pan-cancer EMT-signature identifies RBM47 down-regulation during colorectal cancer progression. *Sci Rep* 7: 4687
- Seshagiri S, Stawiski EW, Durinck S, Modrusan Z, Storm EE, Conboy CB, Chaudhuri S, Guan Y, Janakiraman V, Jaiswal BS et al (2012) Recurrent R-spondin fusions in colon cancer. *Nature* 488: 660–664
- Spit M, Fenderico N, Jordens I, Radaszkiewicz T, Lindeboom RG, Bugter JM, Cristobal A, Ootes L, van Osch M, Janssen E et al (2020) RNF43 truncations trap CK1 to drive niche-independent self-renewal in cancer. *EMBO J* 39: e103932
- Szenker-Ravi E, Altunoglu U, Leushacke M, Bosso-Lefevre C, Khatoo M, Thi Tran H, Naert T, Noelanders R, Hajamohideen A, Beneteau C et al (2018) RSPO2 inhibition of RNF43 and ZNRF3 governs limb development independently of LGR4/5/6. *Nature* 557: 564–569
- Taelman VF, Dobrowolski R, Plouhinec JL, Fuentealba LC, Vorwald PP, Gumper I, Sabatini DD, De Robertis EM (2010) Wnt signaling requires sequestration of glycogen synthase kinase 3 inside multivesicular endosomes. *Cell* 143: 1136–1148
- Tejeda-Munoz N, Albrecht LV, Bui MH, De Robertis EM (2019) Wnt canonical pathway activates macropinocytosis and lysosomal degradation of extracellular proteins. *Proc Natl Acad Sci USA* 116: 10402–10411
- The Gene Ontology Consortium (2019) The Gene Ontology Resource: 20 years and still GOing strong. *Nucleic Acids Res* 47: D330–D338
- Thiery JP, Sleeman JP (2006) Complex networks orchestrate epithelial-mesenchymal transitions. *Nat Rev Mol Cell Biol* 7: 131–142
- Timmins NE, Dietmair S, Nielsen LK (2004) Hanging-drop multicellular spheroids as a model of tumour angiogenesis. *Angiogenesis* 7: 97–103
- Tsukiyama T, Fukui A, Terai S, Fujioka Y, Shinada K, Takahashi H, Yamaguchi TP, Ohba Y, Hatakeyama S (2015) Molecular role of RNF43 in canonical and noncanonical Wnt signaling. *Mol Cell Biol* 35: 2007–2023
- Tsukiyama T, Zou J, Kim J, Ogamino S, Shino Y, Masuda T, Merenda A, Matsumoto M, Fujioka Y, Hirose T et al (2020) A phospho-switch controls RNF43-mediated degradation of Wnt receptors to suppress tumorigenesis. *Nat Commun* 11: 4586
- Vincan E, Darcy PK, Farrelly CA, Faux MC, Brabletz T, Ramsay RG (2007) Frizzled-7 dictates three-dimensional organization of colorectal cancer cell carcinoids. *Oncogene* 26: 2340–2352
- Vogelstein B, Papadopoulos N, Velculescu VE, Zhou S, Diaz Jr LA, Kinzler KW (2013) Cancer genome landscapes. *Science* 339: 1546–1558
- Voloshanenko O, Erdmann G, Dubash TD, Augustin I, Metzger M, Moffa G, Hundsrucker C, Kerr G, Sandmann T, Anchang B et al (2013) Wnt secretion is required to maintain high levels of Wnt activity in colon cancer cells. *Nat Commun* 4: 2610
- Voloshanenko O, Gmach P, Winter J, Kranz D, Boutros M (2017) Mapping of Wnt-Frizzled interactions by multiplex CRISPR targeting of receptor gene families. *FASEB J* 31: 4832–4844
- Wang G, Fu Y, Yang X, Luo X, Wang J, Gong J, Hu J (2016) Brg-1 targeting of novel miR550a-5p/RNF43/Wnt signaling axis regulates colorectal cancer metastasis. *Oncogene* 35: 651–661
- Wang Y, Krivtsov AV, Sinha AU, North TE, Goessling W, Feng Z, Zon LI, Armstrong SA (2010) The Wnt/beta-catenin pathway is required for the development of leukemia stem cells in AML. *Science* 327: 1650–1653
- Zagaria A, Anelli L, Coccaro N, Tota G, Casieri P, Cellamare A, Minervini A, Minervini CF, Brunetti C, Cumbo C et al (2014) 5'RUNX1-3'USP42 chimeric gene in acute myeloid leukemia can occur through an insertion mechanism rather than translocation and may be mediated by genomic segmental duplications. *Mol Cytogenet* 7: 66
- Zebisch M, Jones EY (2015) Crystal structure of R-spondin 2 in complex with the ectodomains of its receptors LGR5 and ZNRF3. *J Struct Biol* 191: 149–155



License: This is an open access article under the terms of the Creative Commons Attribution-NonCommercial-NoDerivs License, which permits use and distribution in any medium, provided the original work is properly cited, the use is non-commercial and no modifications or adaptations are made.